Journal of Applied Physics

# Electronic and optoelectronic properties of van der Waals heterostructure based on graphene-like GaN, blue phosphorene, SiC, and ZnO: A first principles study

Cite as: J. Appl. Phys. **127**, 245302 (2020); https://doi.org/10.1063/5.0011303
Submitted: 20 April 2020 . Accepted: 14 June 2020 . Published Online: 25 June 2020

M. Idrees, Chuong V. Nguyen, H. D. Bui, and Bin Amin



Journal of Applied Physics ARTICLE scitation.org/journal/jap

# Electronic and optoelectronic properties of van der Waals heterostructure based on graphene-like GaN, blue phosphorene, SiC, and ZnO: A first principles study

Cite as: J. Appl. Phys. **127**, 245302 (2020); doi: 10.1063/5.0011303
Submitted: 20 April 2020 · Accepted: 14 June 2020 ·
Published Online: 25 June 2020



M. Idrees,[1] Chuong V. Nguyen,[2,a)] H. D. Bui,[3] and Bin Amin[4,b)]

## AFFILIATIONS

[1]Department of Physics, Hazara University, Mansehra 21300, Pakistan
[2]Department of Materials Science and Engineering, Le Quy Don Technical University, Ha Noi 100000, Viet Nam
[3]Institute of Research and Development, Duy Tan University, Da Nang 550000, Viet Nam
[4]Department of Physics, Abbottabad University of Science and Technology, Abbottabad 22010, Pakistan

[a)]**Author to whom correspondence should be addressed:** chuongnguyen11@gmail.com
[b)]**Electronic mail:** binukhn@gmail.com

## ABSTRACT

The combination of two-dimensional materials in the form of van der Waals heterostructures has been proved to be an effective approach for designing electronic and optoelectronic devices. In this work, we investigate the electronic, optical, and photocatalytic properties of vdW heterostructures based on BlueP, SiC, ZnO, and g-GaN using density functional theory. We find that all the g-GaN based vdW heterostructures are energetically and thermally stable at room temperature. The g-GaN–BlueP and g-GaN–SiC heterostructures show indirect bandgaps with the type-II and type-I band alignments, respectively, whereas the g-GaN–ZnO heterostructure shows a direct bandgap with type-II band alignment. Furthermore, the absorption coefficient is also calculated to understand the optical behavior of these hetrostructures. Our results demonstrate that the lowest energy transitions are dominated by excitons, and the blue shift is also observed in these hetrostructures. The g-GaN–BlueP, g-GaN–SiC, and g-GaN–ZnO vdW heterostructures possess outstanding optical absorption in the visible light. The g-GaN–P shows the highest absorption intensity of $10^5$ cm$^{-1}$, which is larger than that of g-GaN–SiC and g-GaN–ZnO vdW heterostructures by three times. These findings demonstrate that these vdW heterostructures are promising candidates for water splitting in the visible light region. Moreover, the heterostructures also show good response to the photocatalytic properties at pH = 0 and pH = 7.



## I. INTRODUCTION

Following the successful exfoliation of graphene, scientists are motivated for two-dimensional (2D) materials due to their unusual physical properties that will offer distinct features for next generation nanodevices.[1–6] Several 2D materials, such as hexagonal boron nitride (h–BN),[7–9] phosphorene (P),[10] transition metal dichalcogenides (TMDCs),[11] Janus–TMDCs,[12,13] BSe,[14] and silicon carbide (SiC),[15] have been experimentally synthesized and theoretically predicted for various potential applications. Recently, graphene-like gallium nitride (g-GaN) has been fabricated through the migration enhanced encapsulated growth (MEEG).[16] Monolayer g-GaN is a 2D semiconductor with a wide bandgap of about 4 eV.[17] The properties of monolayer g-GaN can enhance by doping, adsorption, and making heterostructures.[18–20] Moreover, it is obvious that the heterostructure between g-GaN and BlueP forms a type-II band alignment, making it a promising application as a photocatalytic.[17,21,22] Besides, Ren *et al.*[20] demonstrated that the g-GaN/BSe heterostructure possesses a type-II band alignment, which can promote the separation of the photogenerated electron–hole pairs constantly. Furthermore, the 2D SiC monolayer with a 2D planar graphene-like

structure has recently emerged as a promising material with large in-plane stiffness, tunable nonmagnetic bandgap, and high carrier mobility.[23] Zhu and Tománek[24] predicted the monolayer BlueP, which gained more interest due to a sizable bandgap and ultra-high mobility.[25] Sun *et al.*[26] demonstrated that the defects can enhance the ability of BlueP to absorb the light. The application of BlueP is also checked in superconductors and thermoelectric materials.[27] Density functional theory (DFT) is also performed to find out the effect of doping, electric field, and surface functionalization in the g-GaN monolayer.[28–32] The ZnO monolayer is also gaining much interest due to its fascinating physical and chemical properties, such as a large exciton binding energy, chemical bonding, and their application in gas sensor and solar cell.[33,34]

Recently, the properties of 2D materials can be tuned by various method, one of them is making their heterostructures.[18] 2D vdW heterostructures have attracted considerable attention because they have enriched diversity of 2D materials and spawned dazzling electronic and optoelectronic devices.[35] The popular and important application of 2D vdW heterostructures is making type-II band alignment.[21,36,37] In type-II vdW heterostructure, the valance band maxima (VBM) and conduction band minima (CBM) come from different monolayers. It indicates that the VBM and CBM of one monolayer is lower than those of the other one. As electron and hole are migrated from lower to higher energy, respectively, after exited they will move to different layers of the stake monolayers. In this process, a unwanted combination of photogenerated electron and hole is produced. Type-II band alignment has been found in many newly designed GeC–Janus heterostructures,[38] BlueP–SiC–BSe heterostructures,[39] Janus–Janus heterostructures,[40] TMDCs–TMDCs heterostructures,[18] SiC–TMDCs heterostructures,[41] and $SnSe_2$–$MoS_2$ heterostructures.[42] Also, all these heterostructures are found to be good photocatalytic materials.

In this work, we investigate the electronic properties of three vertical heterostructures of g-GaN–BlueP, g-GaN–SiC, and g-GaN–ZnO. The interactions in these heterostructures take place through weak vdW forces. The most energetically favorable stacking configuration, electronic band and weighted band structures, band edges, effective masses, charge transfer, planar and average electrostatic potentials, optical absorption, the imaginary part of the dielectric function, as well as the photocatalytic response of these vdW heterostructures will be discussed in detail.

## II. COMPUTATIONAL DETAILS

All the calculations are performed by density functional theory (DFT) with a projector augmented plane wave, which is implemented in Vienna *Ab Initio* Simulation Package (VASP).[43] For geometric optimization, the Grimme vdW correction with a 500 eV cutoff was used in Perdew–Burke– Ernzerhof (PBE)[44] to converge the forces and energy to $10^{-6}$ eV/Å and $10^{-5}$ eV, respectively. We used a $(6 \times 6 \times 1)$ Γ-centered Monkhorst–Pack k-mesh for structural optimization and a $(12 \times 12 \times 1)$ for electronic properties calculations. To avoid the periodic interaction, we add a vacuum layer of 25 Å along the $z$ direction. We also used the Heyd–Scuseria–Ernzerhof (HSE06)[45,46] functional to obtain more accurate bandgaps and band structures of materials.

The thermal stability of g-GaN–BlueP, g-GaN–SiC, and g-GaN–ZnO vdW heterostructures at room temperature is performed by *ab initio* molecular dynamics (AIMD) simulation.[47,48] The constant particle number, volume, and temperature (NVT) ensemble is simulated by adopting the algorithm of Nose with a test sample of a $6 \times 6$ supercell. Test time and time step for the sample are set to be 6 ps and 1 fs, respectively.

The dielectric function of the constituent g-GaN, BlueP, SiC, and ZnO monolayers and their combined heterostructures are calculated by solving the Bethe–Salpeter equation (BSE) on top of the single shot $G_0W_0$ calculation to include the screening and excitonic effects, which are performed on top of the standard DFT method.

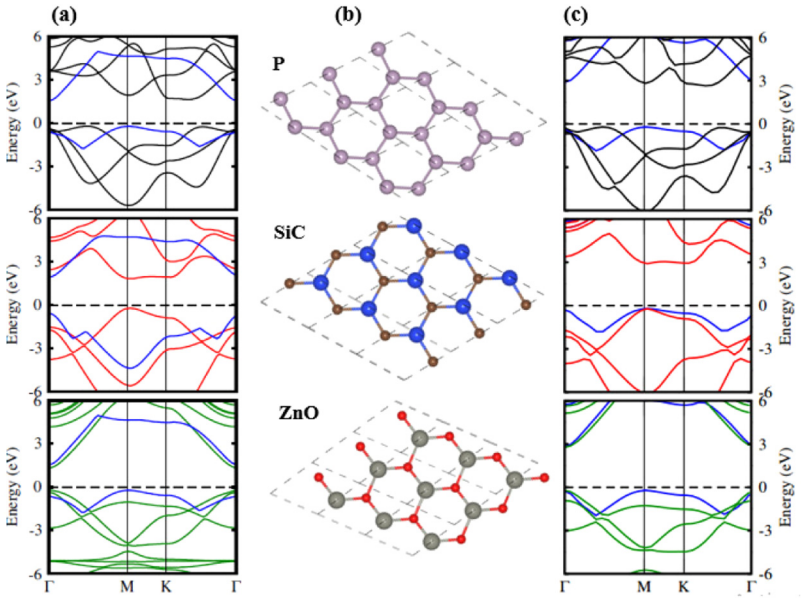


**FIG. 1.** Band structures of g-GaN (blue), BlueP (black), SiC (red), and ZnO (light green) calculated by (a) PBE and (c) HSE04 method. (b) Atomic structures of BlueP, SiC, and ZnO monolayers. The purple balls represent the P atoms. The blue and brown balls represent the Si and C atoms, respectively. The red and gray balls represent the O and Zn atoms, respectively.

**TABLE I.** Binding energies (eV) and interlayer distances (Å) for different stacking configurations of g-GaN–BlueP, g-GaN–SiC, and g-GaN–ZnO vdW heterostructures.

| Heterostructure | g-GaN–BlueP | g-GaN–SiC | g-GaN–ZnO |
|---|---|---|---|
| Stacking-I | −0.111 | −0.108 | −0.126 |
| d | 3.52 | 3.52 | 3.62 |
| Stacking-II | −0.214 | −0.424 | −0.592 |
| d | 3.29 | 3.31 | 3.41 |
| Stacking-III | −0.209 | −0.315 | −0.397 |
| d | 3.60 | 3.44 | 3.45 |
| Stacking-IV | … | −0.179 | −0.592 |
| d | … | 3.58 | 3.54 |
| Stacking-V | … | −0.283 | −0.416 |
| d | … | 3.49 | 3.59 |
| Stacking-VI | … | −0.422 | −0.592 |
| d | … | 3.46 | 3.50 |

## III. RESULTS AND DISSCUSSION

We first check the atomic structure and electronic properties of the constituent g-GaN, BlueP, SiC, and ZnO monolayers. It is found that all these monolayers have hexagonal structures with a relaxed lattice constant of 3.25 Å, 3.27 Å, 3.09 Å, and 3.27 Å for g-GaN, BlueP, SiC, and ZnO monolayers, respectively, which are agreed well with previous results.[39,49] The g-GaN and BlueP monolayers have indirect bandgaps, while the ZnO monolayer is a direct bandgap semiconductor. All the calculated values are agreement with previous results.[39,49] As the electronic properties of 2D materials are sensitive to the strain by making the heterostructures of these monolayers, it will produce compressive and tensile strain in these monolayers. In the g-GaN–BlueP vdW heterostructure, 0.611% and 0% strains are induced in g-GaN and BlueP monolayers, respectively. In the case of g-GaN–SiC and g-GaN–ZnO vdW heterostructures, 1.23%/0.91% and 3.74%/0.30% strains are induced in g-GaN/g-GaN and SiC/ZnO monolayers, respectively. Here, we calculated the electronic band structures of these monolayers with compressive and tensile strains. By inducing these strains, the band structures remain the same while the value of bandgap changes,[50] as plotted in Fig. 1.

For making the vdW heterostructures of g-GaN, BlueP, SiC, and ZnO monolayers, we first check the lattice mismatch of these monolayers. The lattice mismatch of g-GaN–BlueP, g-GaN–SiC, and g-GaN–ZnO is 0.6%, 4.9%, and 0.6%, respectively, which is experimentally achievable.[51] For the g-GaN–BlueP, there are three possible configurations, for g-GaN–SiC six possible configurations; while for g-GaN–ZnO, they have also six possible configurations. Here, we only explained the g-GaN–BlueP possible configurations, as illustrated in Fig. S1 of supplementary material. In stacking (a), BlueP is on the top of the Ga and N atom; in stacking (b), one BlueP atom is in the top of the Ga atom, while the other BlueP is in the hexagonal site; while in stacking (c), one BlueP atom is in the top of the N atom and the other BlueP atom is in the hexagonal site. For all the heterostructures, we calculated the binding energies and interlayer distances to take the most stable configuration and verify their stability. The binding energy is calculated as follows:[49]

$$E_b = E_{total} - E_{1st\ mono} - E_{2nd\ mono}. \quad (1)$$

Here, $E_{total}$, $E_{1st\ mono}$, and $E_{2nd\ mono}$ represent the total energies of the whole system, the first and second monolayers, respectively. From this equation, a negative value means that these heterostructures are energetically stable. Table I shows that the binding energies of g-GaN–BlueP, g-GaN–SiC, and g-GaN–ZnO vdW heterostructures have negative values, hence confirming their stability. We also compare our calculated interlayer distance to that of other typical vdW crystal of graphite, which is about 3.336 Å,[51] as listed in Table I. All the most energetically stable configuration is displayed in Fig. 2 for (a) g-GaN–BlueP, (b) g-GaN–SiC, and (c) g-GaN–ZnO vdW heterostructures, respectively.

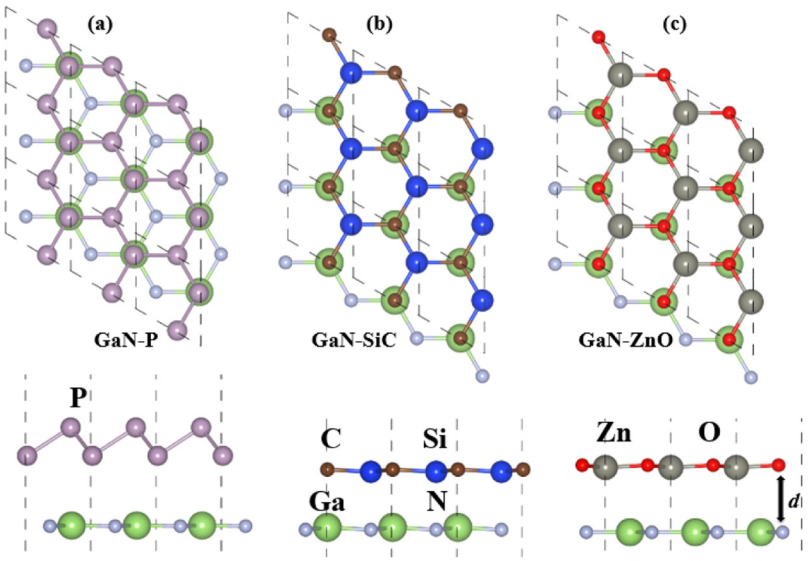


**FIG. 2.** Atomic structures of the most energetically favorable stacking configuration of (a) g-GaN–BlueP, (b) g-GaN–SiC, and (c) g-GaN–ZnO vdW heterostructures. The purple balls represent the P atoms. The blue and brown balls represent the Si and C atoms, respectively. The red and gray balls represent the O and Zn atoms, respectively. The light blue and green balls represent the N and Ga atoms, respectively.

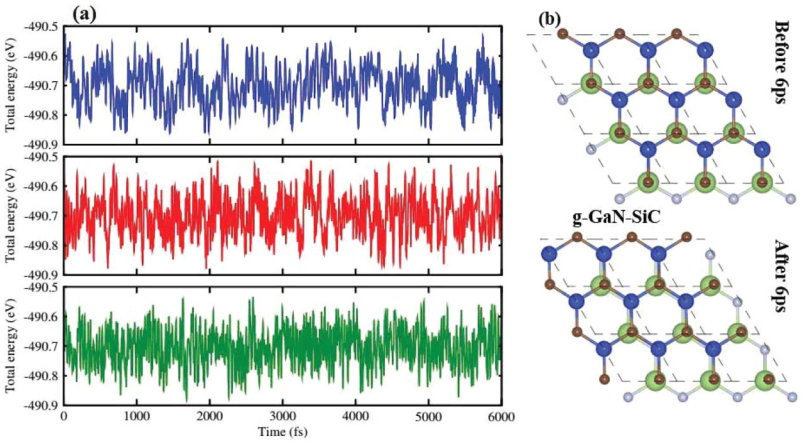


**FIG. 3.** The total energies of (a) g-GaN–BlueP (blue), g-GaN–SiC (red), and g-GaN–ZnO (green) vdW heterostructure as a function of the time under the molecular dynamics simulations at 300 K. (b) represents the g-GaN–SiC vdW heterostructure with no bond-breaking and structural distortion after 6 ps.

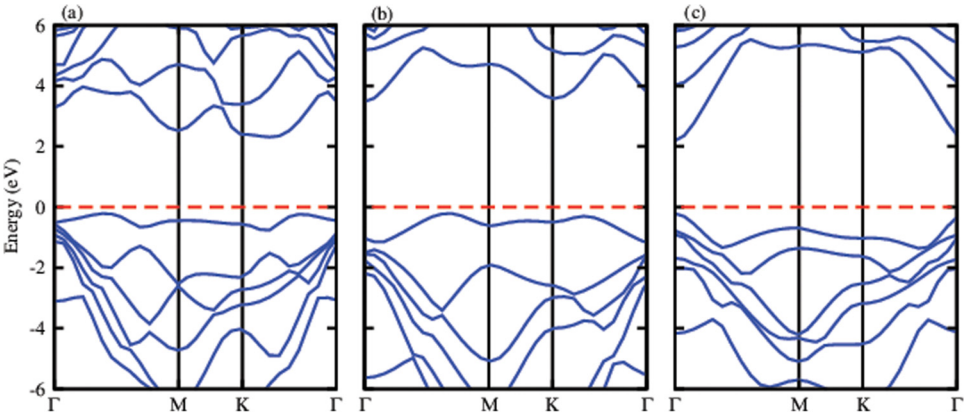


**FIG. 4.** Calculated band structure of (a) g-GaN–BlueP, (b) g-GaN–SiC, and (c) g-GaN–ZnO vdW heterostructure obtained by HSE06 calculation.

Meanwhile, the thermal stability of g-GaN–BlueP, g-GaN–SiC, and g-GaN–ZnO vdW heterostructures is qualitatively tested by AIMD simulation at room temperature. Figure 3(a) shows the fluctuations of total energies for these heterostructures, indicating that the total energy oscillation persistently remains at a fixed value. Moreover, Fig. 3(b) displays that after the AIMD simulation, there is no bond-breaking and structural distortion in the final configurations of these heterostructures. These results imply that the g-GaN–BlueP, g-GaN–SiC, and g-GaN–ZnO vdW heterostructures can be experimentally feasible at room temperature.[52]

## IV. ELECTRONIC PROPERTIES

The projected band structure of g-GaN–BlueP, g-GaN–SiC, and g-GaN–ZnO vdW heterostructures using PBE and HSE06

**TABLE II.** Lattice constant (Å), bond lengths (Å), bandgap (eV), effective masses, work function (eV), conduction, and valence band edges (eV) of the most energetically favorable stacking configuration of g-GaN–BlueP, g-GaN–SiC, and g-GaN–ZnO vdW heterostructures.

| Heterostructure | g-GaN–BlueP | g-GaN–SiC | g-GaN–ZnO |
|---|---|---|---|
| $a$ | 3.27 | 3.21 | 3.28 |
| PBE | 1.7 | 2.6 | 0.84 |
| HSE06 | 2.5 | 3.5 | 2.0 |
| $\Phi$ | 2.05 | 1.86 | 1.59 |
| $m^*_e$ | 0.07 | 0.24 | 0.13 |
| $m^*_h$ | −0.60 | −0.88 | −0.27 |
| $E_{VB}$ | 1.789 | 2.357 | 1.742 |
| $E_{CB}$ | −0.711 | −1.14 | −0.258 |

methods are presented in Fig. S2 of supplementary material and Fig. 4, respectively. One can observe that the upper band structure represents PBE, while the lower one represents the HSE06 calculation. Both PBE and HSE06 band structures depicted in Fig. 4(a) show that the g-GaN–BlueP vdW heterostructure possesses an indirect bandgap semiconductor, which is similar to their monolayers with both the VBM and CBM at the K–Γ path. Similar to g-GaN–BlueP vdW heterostructure depicted in Fig. 4(b), the g-GaN–SiC vdW heterostructure also shows the indirect band nature. If we look to the band nature of g-GaN–ZnO vdW heterostructure, as shown in Fig. 4(c), it exhibits a direct bandgap semiconductor with both VBM and CBM at the Γ-point. All the bandgap values are represented in Fig. 4 and Table II, confirming that all these values are greater than 1.2 eV, showing a good response to photocatalytic.[53]

To check these heterostructures for type-I or type-II band alignment, we have calculated the weighted band structures and partial density of states (PDOS) for g-GaN–BlueP, g-GaN–SiC, and g-GaN–ZnO vdW heterostructures. From Fig. 5, it is clear that g-GaN–BlueP and g-GaN–ZnO vdW heterostructures possess

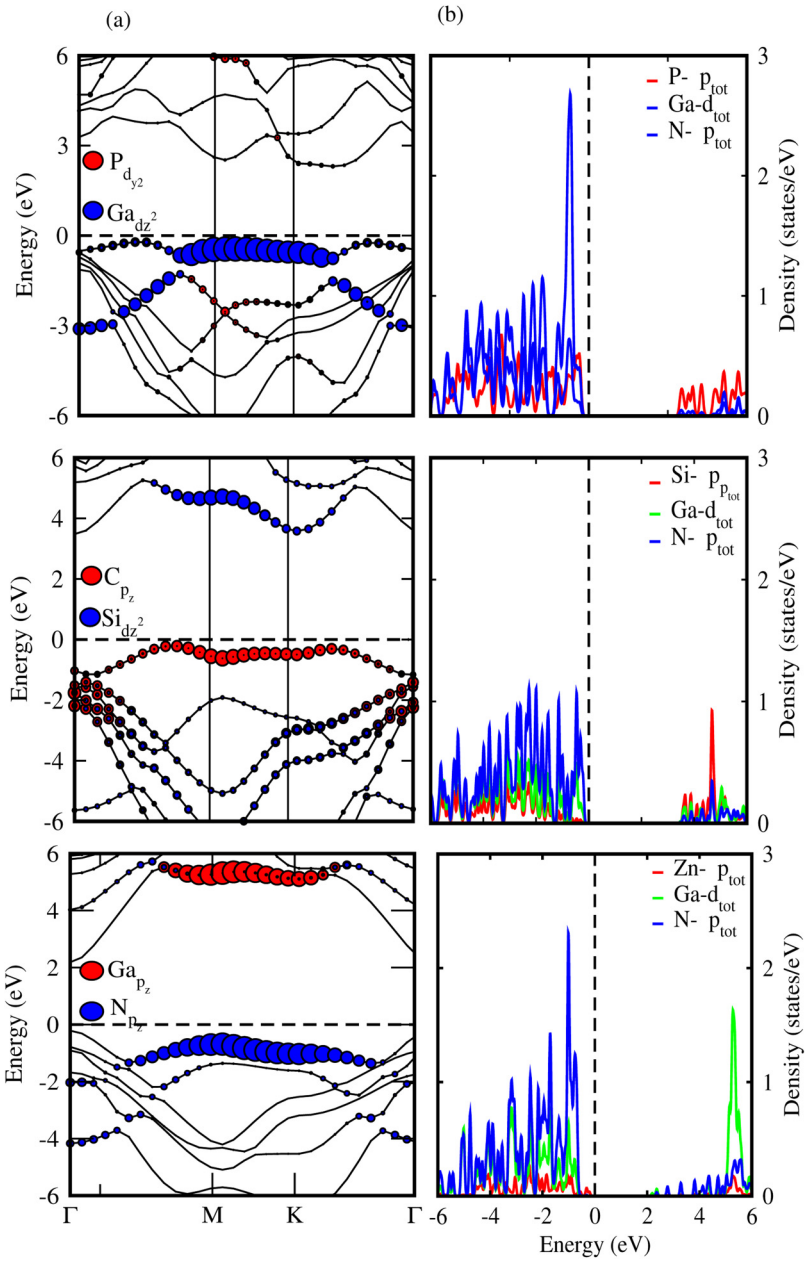


**FIG. 5.** (a) Weighted band structure (left panel) and (b) partial density of states (PDOS) (right panel) of g-GaN–BlueP, g-GaN–SiC, and g-GaN–ZnO vdW heterostructures.

type-II band alignment with VBM from the Ga/N atom and the CBM from the BlueP/Ga atom of the monolayers g-GaN, BlueP, and ZnO, respectively. In type-II band alignment, the free electrons and holes are spontaneously separated, and it shows a good response for optoelectronics and solar energy conversion applications in photovoltaics.[54–56] In the case of g-GaN–SiC heterostructure, both the CBM and VBM are contributed to by the SiC monolayer (VBM is due to the C atom while CBM is due to the Si atom), hence confirming the type-I band alignment. This type of band alignment plays a vital role in optical devices and designing light emitting diodes and laser devices.[57,58] To gain more insight into the physical mechanism of band alignment in the g-GaN based vdW heterostructures, the band decomposed charge density of CBM and VBM is also calculated and plotted in Fig. S3 of supplementary material. In the g-GaN–BlueP (g-GaN–ZnO) vdW heterostructure, the CBM and VBM states are localized on the BlueP (g-GaN) and g-GaN (ZnO) layers, respectively. Thus, photogenerated electrons and holes are confined separately in the two materials, confirming the formation of the type-II band alignment. In the g-GaN–SiC vdW heterostructure, both the CBM and VBM states are localized on the SiC layer. Thus, all the photogenerated electrons and holes are accumulated in the same layer, confirming the formation of the type-I band alignment, which induces the ultrafast recombination of the excited carriers.

To understand the charge transfer between g-GaN–BlueP, g-GaN–SiC, and g-GaN–ZnO vdW heterostructures, we further calculate the charge density difference (CDD) along the z direction, as depicted in Fig. 6. It is clear that for all heterostructures, g-GaN layer donates electrons to the BlueP, SiC, and ZnO monolayers, hence leading to p-doping in g-GaN and n-doping in BlueP, SiC, and ZnO monolayers. We further perform the charge density difference in these heterostructures, which are represented in Fig. 6(a). The total number of electron transfer between g-GaN, BlueP, SiC, and ZnO monolayers is determined by the value of Δ Q(z) at the g-GaN–BlueP, g-GaN–SiC, and g-GaN–ZnO vdW heterostructures interfaces. These results show that the charges of about 0.0054, 0.0157, and 0.0052 *e*/unit cell are transferred from g-GaN to BlueP, SiC, and ZnO layers, respectively. For further confirmation of charge transfer, we also plot the plane-average electrostatic potential along the z direction of the g-GaN–BlueP heterostructure, as shown in Fig. 6(b). One can see that the BlueP layer has a deeper potential than the g-GaN layer, hence driving electrons from the g-GaN layer to the BlueP layer.

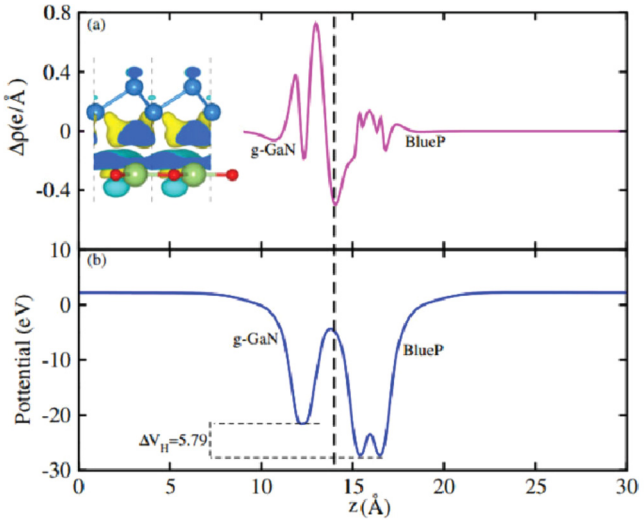


**FIG. 6.** (a) Plane-averaged charge density difference g-GaN–BlueP heterostructure. The inset in (a) is the 3D isosurface of the charge density difference. The yellow and cyan areas represent electrons accumulation and depletion, respectively. (b) Potential profile across the interface of the g-GaN–BlueP heterostructure. The vertical dashed line denotes the heterostructure interface.

The deformation potential theory helps us to calculate the effective mass of materials. Here, we used this theory to check the effective mass for hole and electron of these heterostructures. It is clear that higher carrier mobility is strongly desirable for competent electronic and optoelectronic devices.[59] The effective mass for electron and hole of these heterostructures are listed in Table II, which indicates that the g-GaN–SiC heterostructure has higher carrier mobility than the g-GaN–BlueP and g-GaN–ZnO vdW heterostructures, hence verifying for good optoelectronic devices.[59]

Furthermore, work function Φ is the total amount of energy required to remove electron from the Fermi level. It actually affects the properties of materials and improves the performance of these materials in solar cells. Φ can easily vary by the surface condition of materials, hence altering the surface electric field-induced by the distribution of electrons at the interface.[60] We calculate the Φ along the z direction by aligning the Fermi level to the vacuum level.[61] The calculated values of work functions for g-GaN–BlueP, g-GaN–SiC, and g-GaN–ZnO vdW heterostructures are listed in Table II, which show that g-GaN–BlueP heterostructures have greater values than those of other heterostructures.

## V. OPTICAL PROPERTIES

In this section, we further consider the optical properties of these heterostructures. It is interesting that the dielectric function estimates the response of a material to electromagnetic waves in terms of frequency "$\varepsilon$" as follows:

$$\varepsilon(\omega) = \varepsilon_1(\omega) + i\varepsilon_2(\omega). \tag{2}$$

The above equation contains two parts: one is real and the other one is the imaginary part of dielectric functions. First, we will explain the imaginary part of the dielectric function, as it intimately associated with the band structure. In Fig. 7, we plotted the imaginary part of dielectric function of g-GaN–BlueP, g-GaN–SiC, and g-GaN–ZnO vdW heterostructures, in which the photon energy per eV is plotted against the imaginary part of dielectric functions. We are interested to discuss the peak values of lowest energy transitions that come out to be the first excitonic peak for these strain monolayers and also for heterostructures. The first and second excitonic peaks are represented by "A" and "B" labels for all the isolated monolayers. For all the monolayers, the first exitonic peaks appear on 2 eV, which is dominated by excitons. Similar to corresponding monolayers, the optical transitions for all heterostructures

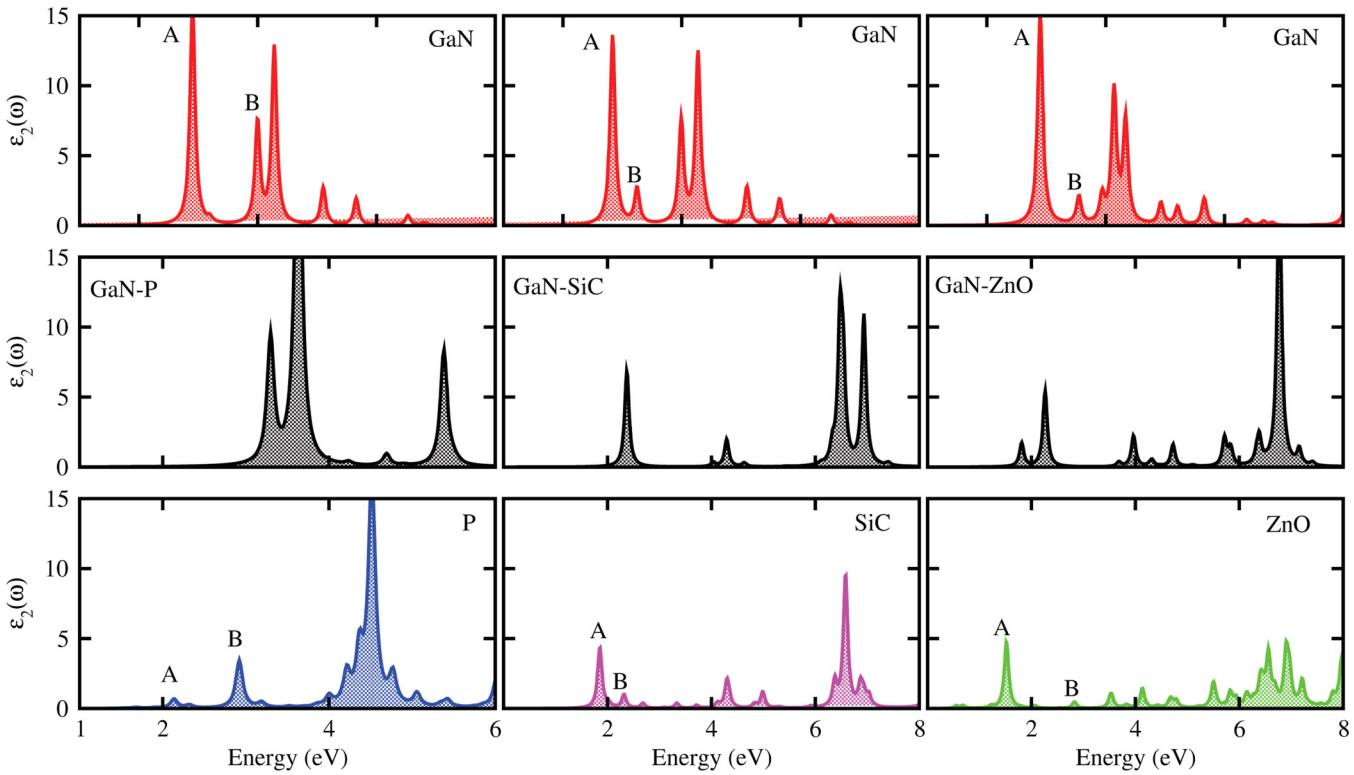


**FIG. 7.** Imaginary part of the dielectric function of induced strain monolayers and g-GaN–BlueP, g-GaN–SiC, and g-GaN–ZnO vdW heterostructures; the names are labels in the figure.

are dominated by excitons. For the g-GaN–BlueP, g-GaN–SiC, and g-GaN–ZnO vdW heterostructures, the first excitonic peak is from higher values than 2 eV, hence shows blue shift. The calculated strain monolayers and g-GaN–BlueP, g-GaN–SiC, and g-GaN–ZnO vdW heterostructures verify good optical absorption in visible regions making them a promising candidate for nanoelectronic and optoelectronic device applications.[62] Furthermore, it is clear that the performances of photocatalytic devices depend strongly on the ability to absorb the light. The optical absorption of g-GaN–BlueP, g-GaN–SiC, and g-GaN–ZnO vdW heterostructures is also calculated and depicted in Fig. 8. One can observe that g-GaN–BlueP, g-GaN–SiC, and g-GaN–ZnO vdW heterostructures possess outstanding optical absorption in the region of visible light. Among these,g-GaN-P shows the highest absorption intensity of $10^5$ cm$^{-1}$, which is larger than that of g-GaN–SiC and g-GaN–ZnO vdW heterostructures by three times. These findings demonstrate that these vdW heterostructures are promising candidates for water splitting in the visible light region.

## VI. PHOTOCATALYTIC PROPERTIES

To check the photocatalytic response at acidic and basic solutions of these heterostructures, we use the Mulliken electronegativity:[63,64] $E_{VBM} = \chi - E_{elec} + 0.5E_g$ and $E_{CBM} = E_{VBM} - E_g$.

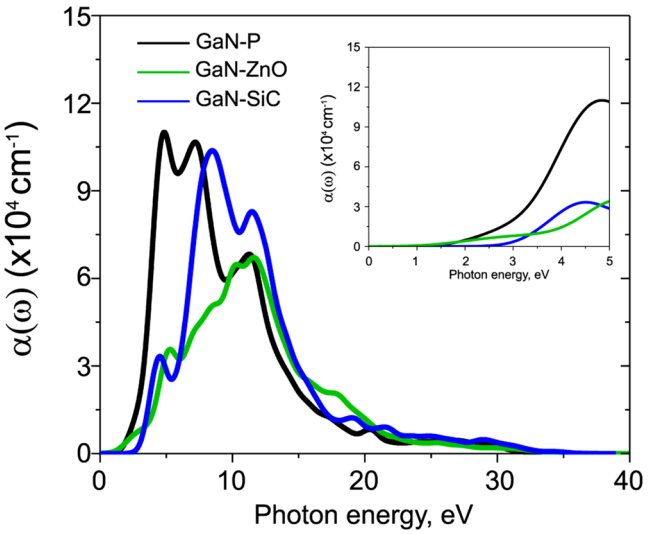


**FIG. 8.** Calculated optical absorption of g-GaN–BlueP, g-GaN–SiC, and g-GaN–ZnO vdW heterostructures as a function of photon energy for the most energetically favorable stacking configuration.

The valence and conduction band edge positions of g-GaN–BlueP, g-GaN–SiC, and g-GaN–ZnO vdW heterostructures for pH = 0 are shown in Fig. 8 and listed in Table II. It is obvious from Fig. 9 that −5.67 (−5.26) eV represents the oxidation potential of water ($E_{O_2/H_2O}$) while −4.44 (−4.03) eV represents the reduction potential of water ($E_{H^+/H_2}$) for pH = 0 (7). One can observe that the band alignments of these heterostructures are insensitive to the change of pH. It indicates that the band edge positions of these vdW heterostructures do not change with the change in pH values. All these heterostructures straddle the redox potential (oxidation and reduction potentials) at pH = 0 and pH = 7 except for g-GaN–ZnO vdW heterostructures, making them suitable for the water splitting reaction. Furthermore, we can find that the redox reactions of the heterostructures occur from different materials. In the case of g-GaN–BlueP heterostructures, water oxidation/reduction takes place from the g-GaN/BlueP layers. To look at the g-GaN–SiC and g-GaN–ZnO vdW heterostructures, the water oxidation and reduction is due to the g-GaN/ZnO and SiC/g-GaN layers. These results show that if we go from pH = 0 to 7, these heterostructures tend to favor for reduction while for oxidation these values decrease.

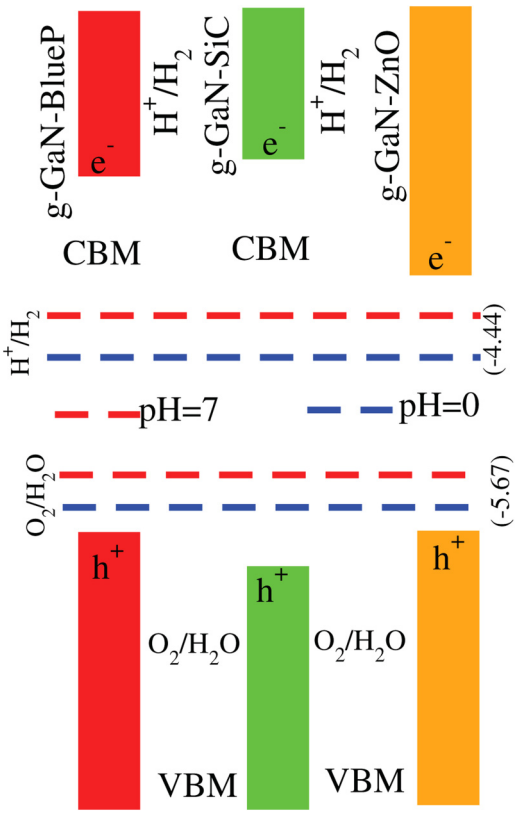


**FIG. 9.** Band alignments of g-GaN–BlueP, g-GaN–SiC, and g-GaN–ZnO vdW heterostructures by the HSE06 calculation with respect to the redox potentials of water.

## VII. CONCLUSION

In summary, we have investigated the structural, electronic, optical, and photocatalytic properties of g-GaN–BlueP, g-GaN–SiC, and g-GaN–ZnO vdW heterostructures using first principles calculations. The electronic and weighted band structures show that g-GaN–BlueP and g-GaN–ZnO vdW heterostructures exhibit type-II band alignment, while the g-GaN–SiC vdW heterostructure shows type-I band alignment. The charge transfer shows that from g-GaN layer, charges are transferred to BlueP, SiC, and ZnO layers. The imaginary part verifies that the excitons dominate the lowest energy transitions in strained monolayers and their vdW heterostructures and also have blue shift in these heterostructures. All the heterostructures show a good response to the photocatalytic properties at pH = 0 and pH = 7.

## SUPPLEMENTARY MATERIAL

See the supplementary material for the Fig. S1: Possible stacking of G-BaN-BlueP vdW; Fig. S2: PBE band structures of all heterostructures; Fig. S3: Band-decomposed charge densities.

## ACKNOWLEDGMENTS

This research is funded by the Higher Education Commission of Pakistan (HEC) under Project No. 5727/KPK/NRPU/R&D/HEC2016 and the Vietnam National Foundation for Science and Technology Development (NAFOSTED) under Grant No. 103.01-2019.05.

## DATA AVAILABILITY

The data that support the findings of this study are available from the corresponding author upon reasonable request.

## REFERENCES

[1]K. S. Novoselov, A. K. Geim, S. Morozov, D. Jiang, M. I. Katsnelson, I. Grigorieva, S. Dubonos, and A. A. Firsov, Nature **438**, 197 (2005).
[2]R. R. Nair, P. Blake, A. N. Grigorenko, K. S. Novoselov, T. J. Booth, T. Stauber, N. M. Peres, and A. K. Geim, Science **320**, 1308 (2008).
[3]Q. H. Wang, K. Kalantar-Zadeh, A. Kis, J. N. Coleman, and M. S. Strano, Nat. Nanotechnol. **7**, 699 (2012).
[4]J. Kang, S. Tongay, J. Zhou, J. Li, and J. Wu, Appl. Phys. Lett. **102**, 012111 (2013).
[5]G. R. Bhimanapati, Z. Lin, V. Meunier, Y. Jung, J. Cha, S. Das, D. Xiao, Y. Son, M. S. Strano, V. R. Cooper *et al.*, ACS Nano **9**, 11509 (2015).
[6]S. Zhang, S. Guo, Z. Chen, Y. Wang, H. Gao, J. Gómez-Herrero, P. Ares, F. Zamora, Z. Zhu, and H. Zeng, Chem. Soc. Rev. **47**, 982 (2018).
[7]C. R. Dean, A. F. Young, I. Meric, C. Lee, L. Wang, S. Sorgenfrei, K. Watanabe, T. Taniguchi, P. Kim, K. L. Shepard *et al.*, Nat. Nanotechnol. **5**, 722 (2010).
[8]N. Alem, R. Erni, C. Kisielowski, M. D. Rossell, W. Gannett, and A. Zettl, Phys. Rev. B **80**, 155425 (2009).
[9]K. H. Lee, H.-J. Shin, J. Lee, I.-Y. Lee, G.-H. Kim, J.-Y. Choi, and S.-W. Kim, Nano Lett. **12**, 714 (2012).
[10]J. L. Zhang, S. Zhao, C. Han, Z. Wang, S. Zhong, S. Sun, R. Guo, X. Zhou, C. D. Gu, K. D. Yuan *et al.*, Nano Lett. **16**, 4903 (2016).
[11]Y. Li, Z. Zhou, S. Zhang, and Z. Chen, J. Am. Chem. Soc. **130**, 16739 (2008).
[12]A.-Y. Lu, H. Zhu, J. Xiao, C.-P. Chuu, Y. Han, M.-H. Chiu, C.-C. Cheng, C.-W. Yang, K.-H. Wei, Y. Yang *et al.*, Nat. Nanotechnol. **12**, 744 (2017).
[13]J. Zhang, S. Jia, I. Kholmanov, L. Dong, D. Er, W. Chen, H. Guo, Z. Jin, V. B. Shenoy, L. Shi *et al.*, ACS Nano **11**, 8192 (2017).

[14]S. Demirci, N. Avazli, E. Durgun, and S. Cahangirov, Phys. Rev. B **95**, 115409 (2017).
[15]S. Lin, J. Phys. Chem. C **116**, 3951 (2012).
[16]Z. Y. Al Balushi, K. Wang, R. K. Ghosh, R. A. Vilá, S. M. Eichfeld, J. D. Caldwell, X. Qin, Y.-C. Lin, P. A. DeSario, G. Stone *et al.*, Nat. Mater. **15**, 1166 (2016).
[17]M. Sun, J.-P. Chou, Q. Ren, Y. Zhao, J. Yu, and W. Tang, Appl. Phys. Lett. **110**, 173105 (2017).
[18]B. Amin, N. Singh, and U. Schwingenschlogl, Phys. Rev. B **92**, 075439 (2015).
[19]K. Ren, S. Wang, Y. Luo, J.-P. Chou, J. Yu, W. Tang, and M. Sun, J. Phys. D Appl. Phys. **53**, 185504 (2020).
[20]K. Ren, Y. Luo, S. Wang, J.-P. Chou, J. Yu, W. Tang, and M. Sun, ACS Omega **4**, 21689 (2019).
[21]K. Ren, S. Wang, Y. Luo, Y. Xu, M. Sun, J. Yu, and W. Tang, RSC Adv. **9**, 4816 (2019).
[22]K. Ren, J. Yu, and W. Tang, J. Appl. Phys. **126**, 065701 (2019).
[23]E. Bekaroglu, M. Topsakal, S. Cahangirov, and S. Ciraci, Phys. Rev. B **81**, 075433 (2010).
[24]Z. Zhu and D. Tománek, Phys. Rev. Lett. **112**, 176802 (2014).
[25]J. Xiao, M. Long, X. Zhang, J. Ouyang, H. Xu, and Y. Gao, Sci. Rep. **5**, 9961 (2015).
[26]M. Sun, J.-P. Chou, A. Hu, and U. Schwingenschlogl, Chem. Mater. **31**, 8129 (2019).
[27]J.-J. Zhang and S. Dong, 2D Mater. **3**, 035006 (2016).
[28]M. Sun, W. Tang, Q. Ren, S.-K. Wang, J. Yu, and Y. Du, Appl. Surf. Sci. **356**, 110 (2015).
[29]M. Sun, Y. Hao, Q. Ren, Y. Zhao, Y. Du, and W. Tang, Solid State Commun. **242**, 36 (2016).
[30]W. Yu, Z. Zhu, C.-Y. Niu, C. Li, J.-H. Cho, and Y. Jia, Nanoscale Res. Lett. **11**, 1 (2016).
[31]Y. Mogulkoc, M. Modarresi, A. Mogulkoc, and Y. Ciftci, Comput. Mater. Sci. **124**, 23 (2016).
[32]L. Zhu, S.-S. Wang, S. Guan, Y. Liu, T. Zhang, G. Chen, and S. A. Yang, Nano Lett. **16**, 6548 (2016).
[33]P. V. Radovanovic, N. S. Norberg, K. E. McNally, and D. R. Gamelin, J. Am. Chem. Soc. **124**, 15192 (2002).
[34]X. Ji, J. Song, T. Wu, Y. Tian, B. Han, X. Liu, H. Wang, Y. Gui, Y. Ding, and Y. Wang, Sol. Energy Mater. Sol. Cells **190**, 6 (2019).
[35]D. Jariwala, T. J. Marks, and M. C. Hersam, Nat. Mater. **16**, 170 (2017).
[36]F. Ceballos, M. Z. Bellus, H.-Y. Chiu, and H. Zhao, ACS Nano **8**, 12717 (2014).
[37]Z. Guan, C.-S. Lian, S. Hu, S. Ni, J. Li, and W. Duan, J. Phys. Chem. C **121**, 3654 (2017).
[38]H. Din, M. Idrees, A. Albar, M. Shafiq, I. Ahmad, C. V. Nguyen, and B. Amin, Phys. Rev. B **100**, 165425 (2019).
[39]M. Idrees, H. Din, S. Khan, I. Ahmad, L.-Y. Gan, C. V. Nguyen, and B. Amin, J. Appl. Phys. **125**, 094301 (2019).
[40]M. Idrees, H. Din, R. Ali, G. Rehman, T. Hussain, C. Nguyen, I. Ahmad, and B. Amin, Phys. Chem. Chem. Phys. **21**, 18612 (2019).
[41]H. Din, M. Idrees, G. Rehman, C. V. Nguyen, L.-Y. Gan, I. Ahmad, M. Maqbool, and B. Amin, Phys. Chem. Chem. Phys. **20**, 24168 (2018).
[42]T. V. Vu, N. V. Hieu, L. T. Thao, N. N. Hieu, H. V. Phuc, H. Bui, M. Idrees, B. Amin, L. M. Duc, and C. V. Nguyen, Phys. Chem. Chem. Phys. **21**, 22140 (2019).
[43]G. Kresse and J. Furthmüller, Phys. Rev. B **54**, 11169 (1996).
[44]J. P. Perdew, K. Burke, and M. Ernzerhof, Phys. Rev. Lett. **77**, 3865 (1996).
[45]J. Heyd, G. E. Scuseria, and M. Ernzerhof, J. Chem. Phys. **118**, 8207 (2003).
[46]J. Paier, M. Marsman, K. Hummer, G. Kresse, I. C. Gerber, and J. G. Ángyán, J. Chem. Phys. **124**, 154709 (2006).
[47]J. D. Gale, J. Chem. Soc., Faraday Trans. **93**, 629 (1997).
[48]J. D. Gale and A. L. Rohl, Mol. Simul. **29**, 291 (2003).
[49]S. Wang, C. Ren, H. Tian, J. Yu, and M. Sun, Phys. Chem. Chem. Phys. **20**, 13394 (2018).
[50]I. Ahmad, S. A. Khan, M. Idrees, M. Haneef, I. Shahid, H. U. Din, S. A. Khan, and B. Amin, Physica B **545**, 113 (2018).
[51]X. Chen, F. Tian, C. Persson, W. Duan, and N.-X. Chen, Sci. Rep. **3**, 3046 (2013).
[52]C. Xia, W. Xiong, J. Du, T. Wang, Y. Peng, and J. Li, Phys. Rev. B **98**, 165424 (2018).
[53]Y. Li, Y.-L. Li, B. Sa, and R. Ahuja, Catal. Sci. Technol. **7**, 545 (2017).
[54]P. Rivera, J. R. Schaibley, A. M. Jones, J. S. Ross, S. Wu, G. Aivazian, P. Klement, K. Seyler, G. Clark, N. J. Ghimire *et al.*, Nat. Commun. **6**, 1 (2015).
[55]Q. Peng, Z. Wang, B. Sa, B. Wu, and Z. Sun, Sci. Rep. **6**, 31994 (2016).
[56]V. D. S. Ganesan, J. Linghu, C. Zhang, Y. P. Feng, and L. Shen, Appl. Phys. Lett. **108**, 122105 (2016).
[57]M. Tangi, P. Mishra, M.-Y. Li, M. K. Shakfa, D. H. Anjum, M. N. Hedhili, T. K. Ng, L.-J. Li, and B. S. Ooi, Appl. Phys. Lett. **111**, 092104 (2017).
[58]M. Z. Bellus, M. Li, S. D. Lane, F. Ceballos, Q. Cui, X. C. Zeng, and H. Zhao, Nanoscale Horiz. **2**, 31 (2017).
[59]Y. Liu, X. Duan, Y. Huang, and X. Duan, Chem. Soc. Rev. **47**, 6388 (2018).
[60]F. Opoku, K. K. Govender, C. G. C. E. Van Sittert, and P. P. Govender, New J. Chem. **41**, 8140 (2017).
[61]X. Peng, F. Tang, and A. Copple, J. Phys. Condens. Matter **24**, 075501 (2012).
[62]A. Moliton and R. C. Hiorns, Pol. Int. **53**, 1397 (2004).
[63]K. Maeda and K. Domen, J. Phys. Chem. Lett. **1**, 2655 (2010).
[64]T. R. Cook, D. K. Dogutan, S. Y. Reece, Y. Surendranath, T. S. Teets, and D. G. Nocera, Chem. Rev. **110**, 6474 (2010).